

Evidence for nodeless superconducting gap in $\text{NaFe}_{1-x}\text{Co}_x\text{As}$ from low-temperature thermal conductivity measurements

S. Y. Zhou,¹ X. C. Hong,¹ X. Qiu,¹ B. Y. Pan,¹ Z. Zhang,¹ X. L. Li,¹ W. N. Dong,¹

A. F. Wang,² X. G. Luo,² X. H. Chen,² and S. Y. Li^{1,*}

¹State Key Laboratory of Surface Physics, Department of Physics,

and Laboratory of Advanced Materials, Fudan University, Shanghai 200433, P. R. China

²Hefei National Laboratory for Physical Science at Microscale and Department of Physics,

University of Science and Technology of China, Hefei, Anhui 230026, China

(Dated: November 11, 2018)

The thermal conductivity of optimally doped $\text{NaFe}_{0.972}\text{Co}_{0.028}\text{As}$ ($T_c \sim 20$ K) and overdoped $\text{NaFe}_{0.925}\text{Co}_{0.075}\text{As}$ ($T_c \sim 11$ K) single crystals were measured down to 50 mK. No residual linear term κ_0/T is found in zero magnetic field for both compounds, which is an evidence for nodeless superconducting gap. Applying field up to $H = 9$ T ($\approx H_{c2}/4$) does not noticeably increase κ_0/T in $\text{NaFe}_{0.972}\text{Co}_{0.028}\text{As}$, which is consistent with multiple isotropic gaps with similar magnitudes. The κ_0/T of overdoped $\text{NaFe}_{0.925}\text{Co}_{0.075}\text{As}$ shows a relatively faster field dependence, indicating the increase of the ratio between the magnitudes of different gaps, or the enhancement of gap anisotropy upon increasing doping.

PACS numbers: 74.70.Xa, 74.25.fc

The discovery of high-temperature superconductivity in iron pnictides^{1,2} has attracted great attentions. Many efforts have been devoted to determine the symmetry and structure of their superconducting gap,³ which is one of the keys to understand the electronic pairing mechanism.⁴

For the most studied $(\text{Ba,Sr,Ca,Eu})\text{Fe}_2\text{As}_2$ (122) system, while multiple nodeless superconducting gaps were demonstrated near optimal doping,⁵⁻⁹ nodal superconductivity was found in the extremely hole-doped KFe_2As_2 ,^{10,11} and highly anisotropic gap⁹ or isotropic gaps with significantly different magnitudes^{12,13} were suggested in the heavily electron-doped $\text{Ba}(\text{Fe}_{1-x}\text{Co}_x)_2\text{As}_2$. Intriguingly, nodal superconductivity was also found in isovalently doped $\text{BaFe}_2(\text{As}_{1-x}\text{P}_x)_2$ and $\text{Ba}(\text{Fe}_{1-x}\text{Ru}_x)_2\text{As}_2$.¹⁴⁻¹⁷

For the two stoichiometric LiFeAs and LiFeP (111) compounds, it was clearly shown that the former has nodeless superconducting gaps,¹⁸⁻²¹ and the latter has nodal gap.²² However, for another 111 compound $\text{NaFe}_{1-x}\text{Co}_x\text{As}$, recently there were controversial experimental results on its gap structure.^{23,24} High-resolution angle-resolved photoemission spectroscopy (ARPES) measurements on $\text{NaFe}_{0.95}\text{Co}_{0.05}\text{As}$ ($T_c \sim 18$ K) unambiguously showed nearly isotropic superconducting gaps on all three Fermi surfaces,²³ but London penetration depth measurements claimed nodal gap in $\text{NaFe}_{1-x}\text{Co}_x\text{As}$ from underdoped to overdoped range (x ranging from 0.02 to 0.10).²⁴ To resolve this important issue, more experiments are highly desired.

The ultra-low-temperature heat transport measurement is a bulk technique to probe the gap structure of superconductors.²⁵ Whether there is a finite residual linear term κ_0/T in zero field is a good judgement on the existence of gap nodes or not. The field dependence of κ_0/T can further give information of nodal gap, gap anisotropy, or multiple gaps.²⁵ During past three years,

thermal conductivity measurements have provided valuable experimental results to clarify the gap structure of iron-based superconductors.²⁶

In this Rapid Communication, we present the thermal conductivity measurements of optimally doped $\text{NaFe}_{0.972}\text{Co}_{0.028}\text{As}$ and overdoped $\text{NaFe}_{0.925}\text{Co}_{0.075}\text{As}$ single crystals down to 50 mK. We find no evidences for gap nodes in both compounds, which supports previous ARPES results in Ref. 23, and disagrees with the penetration depth experiments in Ref. 24. Furthermore, the relatively fast field dependence of κ_0/T in $\text{NaFe}_{0.925}\text{Co}_{0.075}\text{As}$ indicates the increase of the ratio between the magnitudes of those isotropic gaps, or the enhancement of gap anisotropy upon increasing doping. This gap structure evolution is similar to that of $\text{Ba}(\text{Fe}_{1-x}\text{Co}_x)_2\text{As}_2$ system.

The $\text{NaFe}_{1-x}\text{Co}_x\text{As}$ single crystals were synthesized by flux method with NaAs as the flux.²⁷ NaAs was prepared by reacting the Na chunks and As powders in the evacuated quartz tube at 200 °C for 10 hours. Then the powders of NaAs , Fe and Co were mixed together according to the ratio $\text{NaAs:Fe:Co} = 4:1-x:x$. The mixture was placed into an alumina crucible and then sealed inside an iron crucible under Ar atmosphere. The crucible was put in Ar filled tube furnace and slowly heated up to 950 °C and kept for 10 hours, then slowly cooled down to 600 °C at a rate of 3 °C/h. The shining plate-like $\text{NaFe}_{1-x}\text{Co}_x\text{As}$ single crystals with maximum size of $5 \times 5 \times 0.2$ mm³ were obtained. The actual chemical composition of the single crystals is determined by energy-dispersive X-ray spectroscopy. The cobalt contents are $x = 0.028$ and 0.075 , respectively, for the samples with nominal $x = 0.05$ and 0.20 . The dc magnetic susceptibility was measured at $H = 20$ Oe, with zero-field cooled, using a SQUID (MPMS, Quantum Design).

The single crystals were stored and shipped under the environment of inert gas. After exposed in air, the sam-

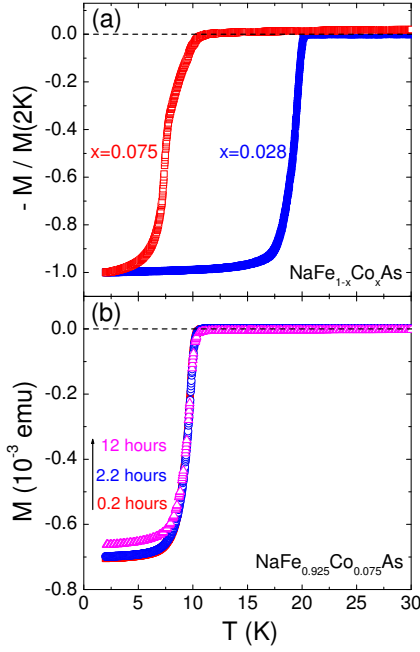


FIG. 1: (Color online). (a) Normalized dc magnetization of $\text{NaFe}_{0.972}\text{Co}_{0.028}\text{As}$ and $\text{NaFe}_{0.925}\text{Co}_{0.075}\text{As}$ single crystals used for transport study. (b) Magnetization of another $\text{NaFe}_{0.925}\text{Co}_{0.075}\text{As}$ single crystal from the same batch, which also has millimeter size in the ab -plane and ~ 100 μm along c -axis, after being exposed in air for 0.2, 2.2, and 12 hours, respectively. The magnetization barely changes during the initial 2.2 hours.

ple was quickly cleaved to a rectangular shape with typical dimensions of $\sim 2.50 \times 1.00$ mm^2 in the ab -plane, and ~ 100 μm along the c -axis. Then four silver wires were attached on the sample with silver paint, which were used for both thermal conductivity and resistivity measurements. The time of exposure in air is less than one hour, before the heat transport study. In-plane thermal conductivity was measured in a dilution fridge using a standard four-wire steady-state method with two RuO_2 chip thermometers, calibrated *in situ* against a reference RuO_2 thermometer. After the thermal conductivity measurements, the sample was quickly (roughly 30 minutes exposure in air) switched to a ^4He cryostat for resistivity measurements. Finally, the contact resistances were examined, with typical value of 100 $\text{m}\Omega$ at 2 K. Magnetic fields were applied along the c -axis. To ensure a homogeneous field distribution in the samples, all fields were applied at temperature above T_c .

Figure 1(a) presents the normalized dc magnetization of $\text{NaFe}_{0.972}\text{Co}_{0.028}\text{As}$ and $\text{NaFe}_{0.925}\text{Co}_{0.075}\text{As}$ single crystals. The onset transition temperatures T_c are 20 and 11 K, respectively. For $\text{NaFe}_{0.972}\text{Co}_{0.028}\text{As}$, the data were taken on a crystal right after being cleaved from the sample used for transport study. For $\text{NaFe}_{0.925}\text{Co}_{0.075}\text{As}$, the data were taken directly on the sample used for transport study, after all transport experiments have been done, totally about 2 hours exposure in air. In order to check

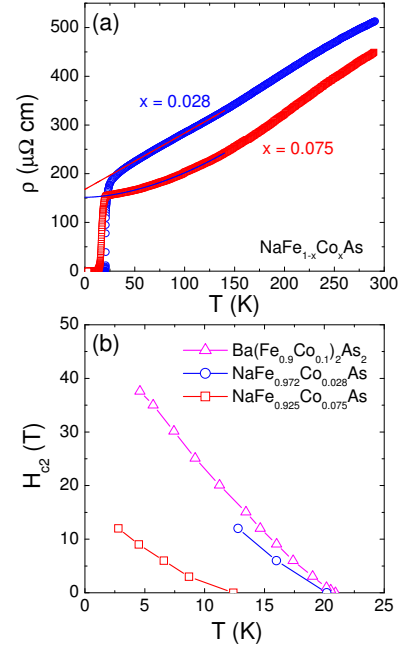


FIG. 2: (Color online). (a) In-plane resistivity of $\text{NaFe}_{0.972}\text{Co}_{0.028}\text{As}$ and $\text{NaFe}_{0.925}\text{Co}_{0.075}\text{As}$ single crystals. The solid lines are linear fit for $\text{NaFe}_{0.972}\text{Co}_{0.028}\text{As}$ between 50 and 140 K, and a fit to $\rho(T) = \rho_0 + AT^n$ for $\text{NaFe}_{0.925}\text{Co}_{0.075}\text{As}$ between 25 and 140 K, respectively. (b) The upper critical field $H_{c2}(T)$ of $\text{NaFe}_{0.972}\text{Co}_{0.028}\text{As}$ and $\text{NaFe}_{0.925}\text{Co}_{0.075}\text{As}$, defined by $\rho = 0$. For comparison, the data of $\text{Ba}(\text{Fe}_{0.9}\text{Co}_{0.1})_2\text{As}_2$ with $T_c \approx 22$ K is also plotted.²⁹

how sensitive is the bulk superconductivity to the exposure time, we measured another $\text{NaFe}_{0.925}\text{Co}_{0.075}\text{As}$ single crystal from the same batch, which also has millimeter size in ab -plane and ~ 100 μm along c -axis. Fig. 1(b) shows its magnetization after being exposed in air for 0.2, 2.2, and 12 hours, respectively. The magnetization barely changes during the initial 2.2 hours, therefore it is concluded that within 2.2 hours there is little effect of air on the bulk superconductivity of $\text{NaFe}_{1-x}\text{Co}_x\text{As}$ single crystals with this kind of size. We notice that the bulk superconductivity degrades faster in air for smaller and thinner single crystals, which is understandable. Since the contact resistances remain low at the end of transport measurements, our resistivity and thermal conductivity data represent the intrinsic properties of the two $\text{NaFe}_{1-x}\text{Co}_x\text{As}$ compounds.

Figure 2(a) shows the in-plane resistivity $\rho(T)$ of $\text{NaFe}_{0.972}\text{Co}_{0.028}\text{As}$ and $\text{NaFe}_{0.925}\text{Co}_{0.075}\text{As}$ single crystals. The T_c defined by $\rho = 0$ are 20.2 and 12.4 K, respectively. This T_c of $\text{NaFe}_{0.925}\text{Co}_{0.075}\text{As}$ sample is about 1 K higher than that determined from magnetization measurement, possibly due to slight inhomogeneity. We name these two samples as OP20K and OD11K. For OP20K, the resistivity data between 50 and 140 K can be fitted linearly, giving a residual resistivity $\rho_0 = 167.8 \pm 0.1$ $\mu\Omega\text{cm}$. For OD11K, the data between 25 and 140 K are fitted to $\rho(T) = \rho_0 + AT^n$, which gives $\rho_0 = 151.6 \pm 0.1$

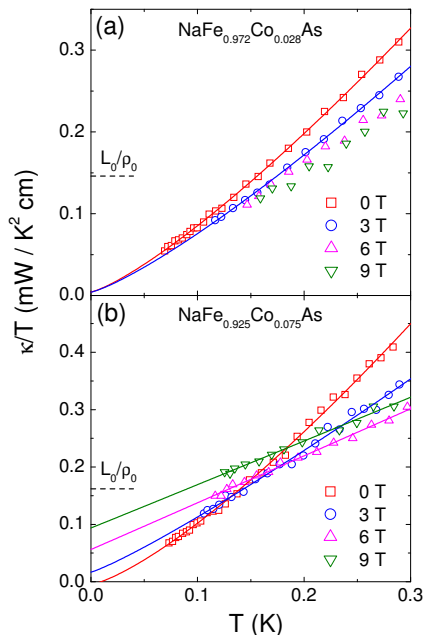


FIG. 3: (Color online). Low-temperature in-plane thermal conductivity of $\text{NaFe}_{0.972}\text{Co}_{0.028}\text{As}$ and $\text{NaFe}_{0.925}\text{Co}_{0.075}\text{As}$ in zero and magnetic fields applied along the c -axis. The solid lines are fits to $\kappa/T = a + bT^{\alpha-1}$. The dash lines are the normal-state Wiedemann-Franz law expectation L_0/ρ_0 , with L_0 the Lorenz number $2.45 \times 10^{-8} \text{ W}\Omega\text{K}^{-2}$ and $\rho_0 = 167.8$ and $151.6 \mu\Omega\text{cm}$, respectively.

$\mu\Omega\text{cm}$ and $n = 1.76 \pm 0.01$. The non-Fermi-liquid linear behavior of $\rho(T)$ near optimal doping, and the increase of power n in the overdoped regime have been observed in $\text{BaFe}_2(\text{As}_{1-x}\text{P}_x)_2$, which was considered as the signature of a quantum critical point.²⁸

The resistivity of these two samples were also measured in magnetic fields up to $H = 12 \text{ T}$, in order to estimate the upper critical field H_{c2} . Fig. 2(b) plots the temperature dependence of H_{c2} for OP20K and OD11K, defined by $\rho = 0$. For comparison, the data of $\text{Ba}(\text{Fe}_{0.9}\text{Co}_{0.1})_2\text{As}_2$ with $T_c \approx 22 \text{ K}$ is plotted.²⁹ From Fig. 2(b), we roughly estimate $H_{c2} \approx 36$ and 15 T for OP20K and OD11K, respectively. To choose a slightly different H_{c2} does not affect our discussion on the field dependence of κ_0/T below.

Figure 3 shows the temperature dependence of in-plane thermal conductivity for OP20K and OD11K in zero and magnetic fields, plotted as κ/T vs T . To get the residual linear term κ_0/T , we fit the curves to $\kappa/T = a + bT^{\alpha-1}$, in which the two terms aT and bT^{α} represent contributions from electrons and phonons, respectively.^{30,31} The power α of the phonon term is typically between 2 and 3.^{30,31} For OP20K in zero field, the fitting gives $\kappa_0/T = a = 0.004 \pm 0.003 \text{ mW K}^{-2} \text{ cm}^{-1}$, with $\alpha = 2.26 \pm 0.03$. For OD11K in zero field, $\kappa_0/T = -0.005 \pm 0.008 \text{ mW K}^{-2} \text{ cm}^{-1}$ and $\alpha = 2.32 \pm 0.06$ are obtained. Previously $\alpha \approx 2.2$ has been observed in BaFe_2As_2 ,³² and $\alpha \approx 2$ was found in $\text{BaFe}_{1.9}\text{Ni}_{0.1}\text{As}_2$ and KFe_2As_2 .^{8,10}

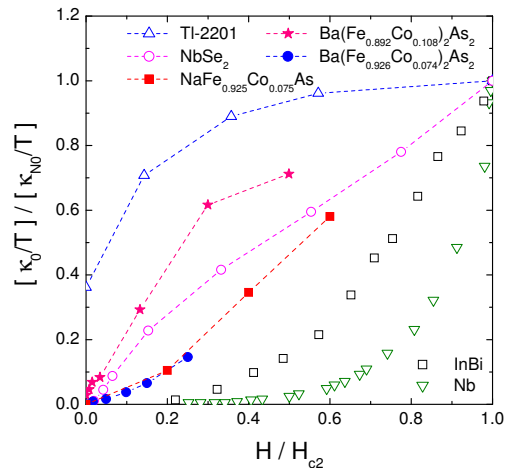


FIG. 4: (Color online). Normalized residual linear term κ_0/T of $\text{NaFe}_{0.925}\text{Co}_{0.075}\text{As}$ as a function of H/H_{c2} . For comparison, similar data are shown for the clean s -wave superconductor Nb,³⁴ the dirty s -wave superconducting alloy InBi,³⁵ the multi-band s -wave superconductor NbSe_2 ,³⁶ an overdoped d -wave cuprate superconductor Tl-2201,³³ the optimally doped $\text{Ba}(\text{Fe}_{0.926}\text{Co}_{0.074})_2\text{As}_2$ and overdoped $\text{Ba}(\text{Fe}_{0.892}\text{Co}_{0.108})_2\text{As}_2$.⁹

Both κ_0/T of OP20K and OD11K in zero field are negligible, within our experimental error bar $\pm 0.005 \text{ mW K}^{-2} \text{ cm}^{-1}$.³¹ In nodeless superconductors, all electrons become Cooper pairs as $T \rightarrow 0$, therefore there are no fermionic quasiparticles to conduct heat and zero κ_0/T is observed, as in the conventional s -wave superconductor V_3Si .³⁰ On the contrary, in a nodal superconductor, the nodal quasiparticles will contribute a finite κ_0/T in zero field, as in the d -wave cuprate superconductor $\text{Tl}_2\text{Ba}_2\text{CuO}_{6+\delta}$ (Tl-2201).³³ Therefore the negligible κ_0/T in both OP20K and OD11K strongly suggest that their superconducting gaps are nodeless. These results are consistent with previous ARPES results in Ref. 23, but disagree with the London penetration depth experiments in Ref. 24.

To gain further support for nodeless gap in OP20K and OD11K, we check the field dependence of their κ_0/T . For OP20K, the fit to the data in $H = 3 \text{ T}$ also gives a negligible $\kappa_0/T = 0.004 \pm 0.011 \text{ mW K}^{-2} \text{ cm}^{-1}$. Further increasing field, the data in $H = 6$ and 9 T become noisy and the fits are not very good, but the tendency is that the κ_0/T does not increase noticeably up to $H = 9 \text{ T}$ ($\approx H_{c2}/4$). This field effect on κ_0/T of OP20K is again consistent with the ARPES experiments on optimally doped $\text{NaFe}_{1-x}\text{Co}_x\text{As}$, which show isotropic gaps with $\Delta_1 = 6.8 \text{ meV}$ for the α hole band and $\Delta_2 = 6.5 \text{ meV}$ for the $\gamma(\delta)$ electron bands.²³ Since the magnitudes of these gaps are very close ($\Delta_1/\Delta_2 = 1.05$), the field effect on κ_0/T is just like that of a superconductor with single isotropic gap,¹³ for examples, the clean s -wave superconductor Nb and the dirty s -wave superconducting alloy InBi, shown in Fig. 4.^{34,35}

As seen in Fig. 3(b), the fits to the thermal con-

ductivity data of OD11K in fields look reliable, so all κ_0/T are obtained up to $H = 9$ T. In Fig. 4, the normalized $(\kappa_0/T)/(\kappa_{N0}/T)$ of OD11K is plotted as a function of H/H_{c2} , with the normal-state Wiedemann-Franz law expectation $\kappa_{N0}/T = L_0/\rho_0 = 0.162$ mW K⁻² cm⁻¹ and $H_{c2} = 15$ T. Similar data of the multi-band *s*-wave superconductor NbSe₂,³⁶ Tl-2201,³³ the optimally doped Ba(Fe_{0.926}Co_{0.074})₂As₂ ($T_c = 22.2$ K) and overdoped Ba(Fe_{0.892}Co_{0.108})₂As₂ ($T_c = 14.6$ K)⁹ are also plotted for comparison. Clearly, the $\kappa_0(H)/T$ behavior of OD11K is very similar to that of optimally doped Ba(Fe_{0.926}Co_{0.074})₂As₂, and much slower than that of overdoped Ba(Fe_{0.892}Co_{0.108})₂As₂.

For optimally doped BaFe_{1.85}Co_{0.15}As₂, the gaps are isotropic, with $\Delta_1 = 6.0$ meV for the β hole pocket and $\Delta_2 = 5.0$ meV for the $\gamma(\delta)$ electron pockets.⁶ The different magnitudes of those gaps ($\Delta_1/\Delta_2 = 1.32$) may result in the relatively fast field dependence of κ_0/T shown in Fig. 4. For overdoped Ba(Fe_{0.892}Co_{0.108})₂As₂, the κ_0/T increases very rapidly even at low field, which has been interpreted as the manifestation of large ratio (> 3) between Δ_1 and Δ_2 ,¹² or highly anisotropic gap.⁹ The similar $\kappa_0(H)/T$ behaviors between OD11K and optimally doped Ba(Fe_{0.926}Co_{0.074})₂As₂ suggest that the ratio Δ_1/Δ_2 has increased from 1.05 in OP20K to ~ 1.3 in OD11K, or some gaps become anisotropic up to 30%. This needs to be checked by the ARPES experiments. From our data, the gap structure evolution upon increasing doping is similar in NaFe_{1-x}Co_xAs

and Ba(Fe_{1-x}Co_x)₂As₂ systems. Note that the field dependence of κ_0/T for OD11K again disagrees with the claim of nodal gap in overdoped NaFe_{1-x}Co_xAs,²⁴ since $\kappa_0(H)/T$ should display a much faster field dependence in that case.

In summary, we have measured the thermal conductivity of optimally doped NaFe_{0.972}Co_{0.028}As and overdoped NaFe_{0.925}Co_{0.075}As single crystals down to 50 mK. The absence of κ_0/T in zero field for both compounds gives strong evidence for nodeless gap. The field effect on κ_0/T of NaFe_{0.972}Co_{0.028}As is consistent with multiple isotropic gaps with similar magnitudes, as demonstrated by ARPES experiments. The relatively faster field dependence of κ_0/T for overdoped NaFe_{0.925}Co_{0.075}As suggests that the different between the magnitudes of those gaps increases, or some gaps become anisotropic upon increasing doping. Our results clearly disagree with the claim of nodal gap in NaFe_{1-x}Co_xAs based on London penetration depth experiments, therefore the issue of gap structure in this 111 system has been clarified.

This work is supported by the Natural Science Foundation of China, the Ministry of Science and Technology of China (National Basic Research Program No: 2009CB929203 and 2012CB821402), and the Program for Professor of Special Appointment (Eastern Scholar) at Shanghai Institutions of Higher Learning.

* E-mail: shiyan_li@fudan.edu.cn

-
- ¹ Y. Kamihara, T. Watanabe, M. Hirano, and H. Hosono, *J. Am. Chem. Soc.* **130**, 3296 (2008).
- ² X. H. Chen, T. Wu, G. Wu, R. H. Liu, H. Chen, and D. F. Fang, *Nature (London)* **453**, 761 (2008).
- ³ P. J. Hirschfeld, M. M. Korshunov, and I. I. Mazin, *Rep. Prog. Phys.* **74**, 124508 (2011).
- ⁴ Fa Wang and Dung-hai Lee, *Science* **332**, 200 (2011).
- ⁵ H. Ding, P. Richard, K. Nakayama, K. Sugawara, T. Arakane, Y. Sekiba, A. Takayama, S. Souma, T. Sato, T. Takahashi, Z. Wang, X. Dai, Z. Fang, G. F. Chen, J. L. Luo, and N. L. Wang, *EPL* **83**, 47001 (2008).
- ⁶ K. Terashima, Y. Sekiba, J. H. Bowen, K. Nakayama, T. Kawahara, T. Sato, P. Richard, Y.-M. Xu, L. J. Li, G. H. Cao, Z.-A. Xu, H. Ding, and T. Takahashi, *Proc. Natl. Acad. Sci.* **106**, 7330 (2009).
- ⁷ X. G. Luo, M. A. Tanatar, J.-Ph. Reid, H. Shakeripour, N. Doiron-Leyraud, N. Ni, S. L. Bud'ko, P. C. Canfield, H. Q. Luo, Z. S. Wang, H.-H. Wen, R. Prozorov, and L. Taillefer, *Phys. Rev. B* **80**, 140503(R) (2009).
- ⁸ L. Ding, J. K. Dong, S. Y. Zhou, T. Y. Guan, X. Qiu, C. Zhang, L. J. Li, X. Lin, G. H. Cao, Z. A. Xu, and S. Y. Li, *New J. Phys.* **11**, 093018 (2009).
- ⁹ M. A. Tanatar, J.-Ph. Reid, H. Shakeripour, X. G. Luo, N. Doiron-Leyraud, N. Ni, S. L. Bud'ko, P. C. Canfield, R. Prozorov, and L. Taillefer, *Phys. Rev. Lett.* **104**, 067002 (2010).
- ¹⁰ J. K. Dong, S. Y. Zhou, T. Y. Guan, H. Zhang, Y. F. Dai, X. Qiu, X. F. Wang, Y. He, X. H. Chen, and S. Y. Li, *Phys. Rev. Lett.* **104**, 087005 (2010).
- ¹¹ K. Hashimoto, A. Serafin, S. Tonegawa, R. Katsumata, R. Okazaki, T. Saito, H. Fukazawa, Y. Kohori, K. Kihou, C. H. Lee, A. Iyo, H. Eisaki, H. Ikeda, Y. Matsuda, A. Carrington, and T. Shibauchi, *Phys. Rev. B* **82**, 014526 (2010).
- ¹² J. K. Dong, S. Y. Zhou, T. Y. Guan, X. Qiu, C. Zhang, P. Cheng, L. Fang, H. H. Wen, and S. Y. Li, *Phys. Rev. B* **81**, 094520 (2010).
- ¹³ Yunkyu Bang, *Phys. Rev. Lett.* **104**, 217001 (2010).
- ¹⁴ Y. Nakai, T. Iye, S. Kitagawa, K. Ishida, S. Kasahara, T. Shibauchi, Y. Matsuda, and T. Terashima, *Phys. Rev. B* **81**, 020503(R) (2010).
- ¹⁵ K. Hashimoto, M. Yamashita, S. Kasahara, Y. Senshu, N. Nakata, S. Tonegawa, K. Ikada, A. Serafin, A. Carrington, T. Terashima, H. Ikeda, T. Shibauchi, and Y. Matsuda, *Phys. Rev. B* **81**, 220501(R) (2010).
- ¹⁶ Y. Zhang, Z. R. Ye, Q. Q. Ge, F. Chen, Juan Jiang, M. Xu, B. P. Xie, and D. L. Feng, arXiv:1109.0229, *Nature Physics* in press.
- ¹⁷ X. Qiu, S. Y. Zhou, H. Zhang, B. Y. Pan, X. C. Hong, Y. F. Dai, Man Jin Eom, Jun Sung Kim, Z. R. Ye, Y. Zhang, D. L. Feng, and S. Y. Li, *Phys. Rev. X* **2**, 011010 (2012).
- ¹⁸ S. V. Borisenko, V. B. Zabolotnyy, D. V. Evtushinsky, T. K. Kim, I. V. Morozov, A. N. Yaresko, A. A. Kordyuk, G. Behr, A. Vasiliev, R. Follath, and B. Büchner, *Phys. Rev. Lett.* **105**, 067002 (2010).
- ¹⁹ M. A. Tanatar, J.-Ph. Reid, S. René de Cotret, N. Doiron-

- Leyraud, F. Laliberté, E. Hassinger, J. Chang, H. Kim, K. Cho, Yoo Jang Song, Yong Seung Kwon, R. Prozorov, and Louis Taillefer, *Phys. Rev. B* **84**, 054507 (2011).
- ²⁰ H. Kim, M. A. Tanatar, Yoo Jang Song, Yong Seung Kwon, and R. Prozorov, *Phys. Rev. B* **83**, 100502(R) (2011).
- ²¹ K. Umezawa, Y. Li, H. Miao, K. Nakayama, Z.-H. Liu, P. Richard, T. Sato, J. B. He, D.-M. Wang, G. F. Chen, H. Ding, T. Takahashi, and S.-C. Wang, *Phys. Rev. Lett.* **108**, 037002 (2012).
- ²² K. Hashimoto, S. Kasahara, R. Katsumata, Y. Mizukami, M. Yamashita, H. Ikeda, T. Terashima, A. Carrington, Y. Matsuda, and T. Shibauchi, *Phys. Rev. Lett.* **108**, 047003 (2012).
- ²³ Z.-H. Liu, P. Richard, K. Nakayama, G.-F. Chen, S. Dong, J.-B. He, D.-M. Wang, T.-L. Xia, K. Umezawa, T. Kawahara, S. Souma, T. Sato, T. Takahashi, T. Qian, Yaobo Huang, Nan Xu, Yingbo Shi, H. Ding, and S.-C. Wang, *Phys. Rev. B* **84**, 064519 (2011).
- ²⁴ K. Cho, M. A. Tanatar, N. Spyrison, H. Kim, G. Tan, P. Dai, C. L. Zhang, and R. Prozorov, arXiv:1201.2966.
- ²⁵ H. Shakeripour, C. Petrovic and L. Taillefer, *New J. Phys.* **11**, 055065 (2009).
- ²⁶ G. R. Stewart, *Rev. Mod. Phys.* **83**, 1589 (2011), and references therein.
- ²⁷ C. He, Y. Zhang, B. P. Xie, X. F. Wang, L. X. Yang, B. Zhou, F. Chen, M. Arita, K. Shimada, H. Namatame, M. Taniguchi, X. H. Chen, J. P. Hu, and D. L. Feng, *Phys. Rev. Lett.* **105**, 117002 (2010).
- ²⁸ S. Kasahara, T. Shibauchi, K. Hashimoto, K. Ikada, S. Tonegawa, R. Okazaki, H. Shishido, H. Ikeda, H. Takeya, K. Hirata, T. Terashima, and Y. Matsuda, *Phys. Rev. B* **81**, 184519 (2010).
- ²⁹ A. Yamamoto, J. Jaroszynski, C. Tarantini, L. Balicas, J. Jiang, A. Gurevich, D. C. Larbalestier, R. Jin, A. S. Sefat, M. A. McGuire, B. C. Sales, D. K. Christen, and D. Mandrus, *Appl. Phys. Lett.* **94**, 062511 (2009).
- ³⁰ M. Sutherland, D. G. Hawthorn, R. W. Hill, F. Ronning, S. Wakimoto, H. Zhang, C. Proust, E. Boaknin, C. Lupien, Louis Taillefer, Ruixing Liang, D. A. Bonn, W. N. Hardy, Robert Gagnon, N. E. Hussey, T. Kimura, M. Nohara, and H. Takagi, *Phys. Rev. B* **67**, 174520 (2003).
- ³¹ S. Y. Li, J.-B. Bonnemaïson, A. Payeur, P. Fournier, C. H. Wang, X. H. Chen, and L. Taillefer, *Phys. Rev. B* **77**, 134501 (2008).
- ³² N. Kurita, F. Ronning, C. F. Miclea, E. D. Bauer, J. D. Thompson, A. S. Sefat, M. A. McGuire, B. C. Sales, D. Mandrus, and R. Movshovich, *Phys. Rev. B* **79**, 214439 (2009).
- ³³ C. Proust, E. Boaknin, R. W. Hill, Louis Taillefer, and A. P. Mackenzie, *Phys. Rev. Lett.* **89**, 147003 (2002).
- ³⁴ J. Lowell and J. B. Sousa, *J. Low. Temp. Phys.* **3**, 65 (1970).
- ³⁵ J. O. Willis and D. M. Ginsberg, *Phys. Rev. B* **14**, 1916 (1976).
- ³⁶ E. Boaknin, M. A. Tanatar, J. Paglione, D. Hawthorn, F. Ronning, R. W. Hill, M. Sutherland, Louis Taillefer, J. Sonier, S. M. Hayden, and J. W. Brill, *Phys. Rev. Lett.* **90**, 117003 (2003).